Applied Catalysis B: Environmental 307 (2022) 121207

Contents lists available at ScienceDirect

Applied Catalysis B: Environmental

journal homepage: www.elsevier.com/locate/apcatb

Regulating oxygen defects via atomically dispersed alumina on Pt/WO_x catalyst for enhanced hydrogenolysis of glycerol to 1,3-propanediol

Man Yang [a,*], Keying Wu [a], Shaodong Sun [a], Yujing Ren [b,*]

[a] School of Materials Science and Engineering, Xi'an University of Technology, Xi'an 710048, Shaanxi, People's Republic of China
[b] School of Life Sciences, Northwestern Polytechnical University, Xi'an 710072, Shaanxi, People's Republic of China

ARTICLE INFO

Keywords:
Glycerol hydrogenolysis
1,3-propanediol
Pt/WO_x
Defects engineering
Atomically dispersed alumina promoter

ABSTRACT

Tungsten-based catalyst has been widely investigated in the field of selective hydrogenolysis of secondary C—O bond, such an important yet challenging strategy, in glycerol conversion, in which the product 1,3-propanediol (1,3-PDO) is of great value in polyester industry. Unfortunately, though it has been proved to be highly active, the identification of the intrinsic tungsten oxide active sites still remains unrevealed to date due to its complex microstructure. Herein, we incorporate atomically dispersed alumina as promoter in the context of the selective hydrogenation of glycerol and report a Pt/Al-WO_x catalyst. This catalyst decidedly outperforms the unpromoted Pt/WO_x, which elevates the 1,3-PDO yield to 2 times. Spectroscopy characterizations and chemisorption experiments have revealed that the high activity and selectivity of Pt/Al-WO_x catalyst results from the more oxygen vacancies on WO_x in-situ generation by the acceleration of atomically dispersed alumina in hydrogen atmosphere, which increases the selective adsorption of glycerol and the in-situ Brønsted acid sites for the selective activation of secondary C—O bonds, thus largely augmenting the hydrogenolysis performance. This discovery not only provides the new strategy of defect engineering to enhance hydrogenolysis performance of secondary C—O bond in biomass compounds, but reveals the unique role of the unsaturated coordination structure of WO_x in chemoselective hydrogenolysis reactions.

1. Introduction

The fast development of biodiesel has brought a huge amount of surplus glycerol in the past decade. The low cost and excess supply of glycerol calls for a value-added convert route in biodiesel industry [1–5]. 1,3-PDO is an important polymer precursor for polyester industry, especially for highly quality polyester polypropylene terephthalate (PTT), thus the selective hydrogenolysis of glycerol to 1,3-PDO has been an attractive research [6–12]. However, it is challenging for targeted cleavage of the secondary C—O bond in glycerol because of the steric hindrance and unfavorable thermodynamics. Thus, it is crucial to develop effective catalyst achieving a high yield of 1,3-PDO.

Pt-WO_x based catalyst is a typical catalyst that is effective for the hydrogenative transformation of glycerol to 1,3-PDO and promising for practical applications, which has become a research focus in recent years [13–23]. The previous studies have shown that the catalytic performance of Pt-WO_x based catalyst is generally affected by the third component considerably [24–28]. For instance, Kurosaka et al. found that Al-MCM-41, SiO_2-A_2O_3, Al_2O_3, anatase TiO_2, zeolite H-Y, and ZrO_2 supported Pt/WO_x catalysts displayed completely different catalytic performance, which was attributed to the different interaction between tungsten oxide and supports. Among all supports, Pt/WO_3/ZrO_2 performed the highest 1,3-PDO selectivity of 24.2% at 85.8% glycerol conversion [29]. Recently, Zong et al. further reported that the Pt/WO_x/tetrahedral ZrO_2 catalyst was far more active and selective than Pt/WO_x/monoclinic ZrO_2 catalyst, because Pt dispersion and Brønsted acid sites could be improved greater on tetrahedral ZrO_2, which were responsible for the 1,3-PDO formation [30]. Ma et al. added appropriate Mn promoter into Pt/WO_x/ZrO_2 catalyst to modify the polymerization degree of WO_x domains. With the doping of Mn, a large amount of medium polymerized WO_x was generated, and strong Brønsted acid sites are found to form when medium polymerized WO_x is interacted with Pt particle, which is proportional to the formation rate of 1,3-PDO [31]. Kaneda et al. reported that Pt/WO_x/AlOOH catalyst gave rise to superior activity and selectivity, and the glycerol conversion and 1,3-PDO selectivity achieved 100% and 66%, respectively [18]. Compared with Al_2O_3 support, the abundant surface hydroxyl groups on AlOOH were

* Corresponding authors.
E-mail addresses: myang@xaut.edu.cn (M. Yang), renyj@nwpu.edu.cn (Y. Ren).

https://doi.org/10.1016/j.apcatb.2022.121207
Received 8 November 2021; Received in revised form 7 February 2022; Accepted 9 February 2022
Available online 12 February 2022

considered to play an important role for the absorption of glycerol [18, 32]. The similar conclusion has also been drawn by Liu et al. on Pt/WAlSi catalyst system [33]. The Kaneda group also reported that Pt nanoparticles-AlO_x/WO_3 catalysts that were prepared by co-impregnation method gave rise to excellent 1,3-PDO yield of 40%. The superior performance was also ascribed to the Al-OH species of only a little amount of AlO_x, which was, however, not sufficiently supported by the data provided [34]. Wang et al. first proposed that Au could act as an effective promoter in Pt-WO_x based catalyst. In the studies, in-situ formed Brønsted acid were testified responsible for the catalytic activity. A great promotion of in-situ generated Brønsted acid sites and an overwhelming selectivity towards 1,3-PDO were achieved after Au incorporation [35,36].

Although the activity and 1,3-PDO selectivity were enhanced markedly by third component additives, the results fall short of providing design principles to construct of Pt-WO_x catalyst, because the precise identification for active structures of WO_x and the origin of Brønsted acids remains ambiguous and even in much debate. WO_x is generally believed to provide intrinsic Brønsted acid sites or in-situ generate proton via spillover hydrogen from the noble metals, resulting in the enhancement of catalytic performance [37]. However, the complex catalyst structure and properties, such as the dispersion and acidity of WO_x, the dispersion of noble Pt, and the interaction between Pt and WO_x, result in addition challenges for the in-depth understanding of the crucial role of tungsten species. For instance, in the studies of García-Fernández et al., Zhu et al. and Wang et al., they believed the medium-degree polymerization of WO_x in Pt/WO_x/Al_2O_3 catalysts was the active sites rather than monodispersed or 3D nanocluster WO_x, which could delocalize the negative charge more easily to require for the more Brønsted acid sites [19,38,39]. They also demonstrated the interaction between Pt and WO_x species was responsible for the 1,3-PDO yield. However, Ma et al. fabricated WPt/SiO_2 catalysts, and the theoretical calculation suggested that the dimeric WO_x could provide more Brønsted acid sites [40]. The WO_x with low-degree polymerization was also investigated by Zong and co-workers. They proposed that the isolated WO_4 in Pt/W-SBA-15 exhibited a superior activity and 1,3-PDO selectivity than polytungstates, the resulting Pt/W-SBA-15 (W/Si=1/640) exhibited 1,3-PDO selectivity of 70.8% even at a high glycerol conversion of 86.8% [22]. Liu et al. also constructed isolated WO_4 species on Al_2O_3 support, after loading noble Pt, the catalyst showed an excellent catalytic performance in glycerol hydrogenolysis [41]. These suggested the dispersion of WO_x is not the intrinsic factor for WO_x that affects the reaction performance. Undoubtedly, WO_x species play a crucial role in the cleavage of glycerol secondary C—O bond, however, what the active site is and how the active site performs still need to be investigated in depth.

Herein, we addressed this challenge in the context of selective hydrogenation of glycerol and now report a catalyst by incorporating atomically dispersed AlO_x onto WO_x support that is synthesized by hydrothermal method followed by deposition of Pt. The structure characterizations show that the addition of AlO_x will not affect the dispersion of Pt and WO_x. Our investigation illustrates that atomically dispersed AlO_x can enhance the 1,3-PDO yield to 2 times. Multi-technique characterization data show that the atomically dispersed AlO_x are associated with oxygen vacancies on tungstate formation in a hydrogen atmosphere that will facilitate the adsorption of 1° -OH of glycerol and the formation of in-situ Brønsted acid, leading to a high catalytic activity and selectively. This work for the first time demonstrates the importance of appropriate increasing oxygen vacancies of tungstate in the Pt-WO_x catalysts for the effective hydrogenolysis of glycerol to 1,3-PDO, and proposes the importance of the unsaturated coordination structure of WO_x for glycerol hydrogenolysis.

2. Experimental

2.1. Chemicals

Ammonium metatungstate (AMT, Aladdin, >99%), Nitric acid (HNO_3, Sinopharm, 65.0~68.0%), ethanol (C_2H_5OH, Tianjin Fuyu Fine Chemical Co., Ltd., AR), Aluminum nitrate nonahydrate ($Al(NO)_3{\cdot}9H_2O$, Aladdin, AR, 99%), Chloroplatinic acid hexahydrate ($H_2PtCl_6{\cdot}6H_2O$, Tianjin Fengchuan Chemical Reagent Technologies Co., Ltd., AR), glycerol ($C_3H_8O_3$, Aladdin, AR), 1–butanol (C_4H_9OH, Sinopharm, >99%). All chemicals were used as received directly without further purification. Ultrapure water with a resistivity of 18.2 $M\Omega{\cdot}cm^{-1}$ was used throughout the experiments.

2.2. Catalyst preparation

Al-WO_3 samples were prepared by hydrothermal method and adsorption method. 3 g AMT was put into 20 mL deionized water and stirred until it was completely dissolved. A solution of HNO_3 was added under stirring until the solution reached a pH value of approximately 0.0. Then, the solution was transferred into a Teflon-lined autoclave and heated at 443 K in an oven for 15 h. After cooling down to room temperature, the yellow solid was separated and put into 30 mL mixed solution of water and ethanol followed by addition of $Al(NO)_3{\cdot}9H_2O$ with stirring for 4 h. After the filtration and drying at 363 K for 12 h, the sample was calcined at 773 K in air for 3 h. The as-prepared Al-WO_3 supports are denoted as yAl-WO_3, in which y represents the weight percentage of Al.

The Pt/yAl-WO_x catalysts were prepared with incipient wetness impregnation method. The as-prepared yAl-WO_3 samples were impregnated with an aqueous solution of $H_2PtCl_6{\cdot}6H_2O$. After drying at 393 K for 12 h, the sample was calcined in air at 573 K for 3 h followed by reduction at 573 K in flowing H_2 for 1 h and passivation with 1% (v/v) O_2/N_2 at room temperature for 4 h. The theoretical loading of Pt was 2.0 wt%.

2.3. Reaction tests

The hydrogenolysis of glycerol was performed in 50 mL autoclave with Teflon lining. Glycerol aqueous solution (12 g, 5 wt%) and catalyst (300 mg) were put into the autoclave and purged with hydrogen several times. Unless otherwise specified, the reaction was conducted at 433 K and initial 3 MPa H_2 for 12 h, while stirring at 800 r/min. The gaseous and liquid products were collected and analyzed separately by a gas chromatograph (GC, Thermo Scientific TRACE 1300) equipped with a flame ionization detector (FID). A DB-WAX capillary column (diameter 0.320 mm, film 0.50 μm, length 30 m) was used for separation.1–butanol was employed as internal standard. The conversion of glycerol and the selectivity of specific product were calculated using the following equations:

$$X_{\text{glycerol}}\,(\%) = (\text{mol}_{\text{glycerol consumed}}) / (\text{mol}_{\text{glycerol fed}}) * 100 \quad (1)$$

$$S_{\text{specific product}}\,(\%) = (\text{mol}_{\text{carbon in specific product}}) / (\text{mol}_{\text{carbon in consumed glycerol}}) * 100 \quad (2)$$

$$Y_{\text{specific product}}\,(\%) = X_{\text{glycerol}}\,(\%) * S_{\text{specific product}}\,(\%) * 100 \quad (3)$$

$$S_{\text{others}}\,(\%) = 100 - \Sigma(S_{1,3\text{-PDO}} + S_{1,2\text{-PDO}} + S_{1\text{-PO}} + S_{2\text{-PO}}) \quad (4)$$

2.4. Catalyst characterization

Nitrogen adsorption-desorption measurements were performed at 77 K on a Micromeritics ASAP 2460 instrument. The specific surface areas (S_{BET}) were calculated from the N_2 adsorption isotherm with BET

equation, and the pore size distributions were obtained using desorption branch of the isotherms and BJH method. Before the physisorption measurements, the sample was firstly dehydrated at 393 K for 1 h and then degassed at 573 K for at least 4 h.

Scanning electron microscope (SEM) images were recorded on a JEOL (JSM-7000F) instrument operated at 15 kV and equipped with EDS microanalysis system.

High resolution transmission electron microscopy (HRTEM) and high-angle annual dark-filed scanning transmission electron microscopy (HAADF-STEM) images were recorded on a JEM-2100F instrument operated at 200 kV and equipped with EDS microanalysis system. The samples were dispersed by ultrasound in ethanol solution for 10 min and dropped onto a holey C/Cu TEM grid.

The power X-ray diffraction (XRD) patterns were acquired on a PW3040/60 X'Pert PRO (PANalytical) diffractometer equipped with a Cu Kα radiation source (λ=0.15432 nm) operated at 40 kV and 40 mA.

X-ray photoelectron spectra (XPS) were recorded on an ESCALAB 250 X-ray photoelectron spectrometer with monochromated Al Kα anode. All binding energies were calibrated for surface charging by referencing them to the energy of the C1s peak at 284.6 eV. Before XPS spectra record, the samples were treated in hydrogen at 573 K for 1 h, and then transferred without exposure to air for data collection.

Raman spectra were recorded using a Horiba Jobin-Yvon Labram-HR800 Raman spectrometer (Raman, Paris, France) equipped with a He-Ne laser (532 nm) with a resolution better than 2 cm^{-1}. Before Raman spectra record, the samples were reduced in hydrogen at 573 K for 1 h, and then passivated with 1% (v/v) O_2/N_2 at room temperature for 4 h.

UV–vis diffuse reflectance spectra (DRS) were obtained on a cintra (GBC) apparatus equipped with an integrated sphere attachment with $BaSO_4$ as the reference. Before UV–vis spectra record, the samples were reduced in hydrogen at 573 K for 1 h, and then passivated with 1% (v/v) O_2/N_2 at room temperature for 4 h.

Temperature-programmed reduction of hydrogen (H_2-TPR) were conducted on an Auto Chem II 2920 apparatus. The sample (~100 mg) was loaded into a U-shape quartz reactor and pretreated with Argon at 423 K for 1 h to remove adsorbed hydrates and carbonates. After cooling down to 193 K, the flowing gas was switched to 10% (v/v) H_2/Ar and the samples were heated to 1073 K at a 10 K/min ramping rate. The amount of H_2 consumption was measured by a thermal conductivity detector (TCD), while a cold trap (a mixture of isopropanol and liquid nitrogen) was placed before TCD to remove generated water. The oxygen defect of WO_x was represented as (3-x) in Pt/Al-WO_x, which was calculated using the following equation.

$$(3\text{-}x) = \frac{\left(\mathrm{mol}\cdot g^{-1}{}_{\text{hydrogen consumption}(193K\sim 573K)}\text{-}2\mathrm{mol}\times\frac{1g\times 2\%_{Pt}}{M_{Pt}}\right)}{(1-2\%_{Pt})g/M_{WO_3}} \quad (5)$$

H_2 chemisorption and temperature-programmed desorption of NH_3 (NH_3-TPD) were conducted on a Micromeritics AutoChem II 2920 chemisorber. Prior to H_2 chemisorption measurements, all the samples were pre-reduced at 573 K under a stream of pure H_2 for 1 h, and then purged under Ar flow for 30 min at 583 K. After being cooled down to 323 K, the flowing gas was switched to a 10% (v/v) H_2/Ar for H_2 chemisorption until saturation was reached. The consumed H_2 were detected with TCD and the H_2-chemisorption were calculated by calibration with the standard sample.

In NH_3-TPD measurement, the samples were pre-reduced in flowing pure H_2 at 573 K for 1 h, and then purged under He flow for 30 min at 583 K. Then the sample was cooled down to 393 K to be ready for pulse adsorption. After adsorption saturation, the samples were heated from 393 K to 1073 K in He flow at a temperature rate of 10 K/min, and the desorbed NH_3 was monitored by a mass spectrometer system. In the measurement, m/e =16 was detected to analyze the desorbed NH_3 to avoid the interference of water.

The attenuated total reflection infrared (ATR-IR) spectroscopy was acquired with a BRUKER Equinox 55 spectrometer equipped with a DLaTGS detector. Before the experiment, the samples were dispersed in ethanol and treated with ultrasound for 1 h. Then, the suspension was dropwise onto the diamond crystal surface on the instrument at the 333 K and dried for 3 h. Before data collection, background spectrum was recorded. And then, to get the signal of the adsorbed substrates, the substrate aqueous solution (5 wt.%) was added dropwise the catalysts surface.

Pyridine-adsorbed Fourier transform infrared (Py-IR) spectra of self-supporting wafers were recorded in the region of 400–4000 cm^{-1} on a Tensor 27 instrument with a resolution better than 2 cm^{-1}. Prior to measurements, about 100 mg samples were evacuated under vacuum at 573 K for 1 h and then cooled down to room temperature (~323 K). After that, pyridine vapor was introduced to the sample for adsorption until saturation. Then, physisorbed pyridine was allowed to evacuate for 30 min followed by reheating to 423 K and recording of the spectra after pyridine chemisorption. Reference spectra were collected at 423 K.

CO-diffuse reflectance infrared Fourier transform (CO-DRIFT) spectra were collected by using a Thermo Scientific Nicolet iS50 spectrometer equipped with an MCT detector. The spectrum was obtained by collecting 32 scans at a resolution of 4 cm^{-1} at temperature of 298 K. A certain amount of a powder sample was loaded into the cell with a ZnSe window which can work at high temperature. For each experiment, the sample was in-situ reduced under 10% (v/v) H_2/He flow with a rate of 30 mL min^{-1} for 1 h at 573 K. After purged with He and cooled to 298 K, the background spectrum was recorded and subsequently the mixture gas of 5% (v/v) CO/He was introduced for collecting CO absorption spectrum.

The ^{1}H-nuclear magnetic resonance (^{1}H NMR) was conducted on a Bruker AV III 400 apparatus. Before the measurement, a certain amount of Pt/Al-WO_x catalyst (around 1 g) was reduced at 573 K in flowing H_2 for 1 h. And the corresponding exhaust gas was injected into dimethylsulfoxide-d6 (DMSO-D6) with specific mass (around 5 g) for collecting generated water. After that the H_2O-containing DMSO-D6 solution was tested by ^{1}H NMR. The amount of generation H_2O was determined by the external standard method.

Table 1
Textural parameters of the WO_3, 0.1Al-WO_3, Pt/WO_x and Pt/0.1Al-WO_x samples.

Samples	S_{BET} (m^2g^{-1})	V_{pore} (cm^3g^{-1})	D_{pore} (nm)	Pt size (nm)		Eg (eV)
				XRD	STEM	
WO_3	6.5	0.03	16.0	–	–	2.67
0.1Al-WO_3	5.9	0.03	21.2	–	–	2.67
Pt/WO_x	8.1	0.04	16.7	3.0	3.2	2.47
Pt/0.1Al-WO_x	8.1	0.04	17.8	3.0	3.0	2.34

3. Results and discussions

3.1. Catalyst synthesis and structure characterization

The AlO_x promoter was anchored to WO_x by adsorption of aqueous aluminum nitrate followed by calcination. Then the metal Pt was loaded by incipient wetness impregnation method. By inductively coupled plasma optical emission spectroscopy (ICP–OES), we confirmed the existence of Al species and the actual Pt and Al loadings (Table S1). The resultant catalyst is denoted as Pt/0.1Al-WO_x, in which the loading of Pt is 2.0 wt.% and the loading of Al is 0.1 wt.% with a W/Al atomic ratio of 114.

The N_2 adsorption-desorption isotherms of the WO_3, 0.1Al-WO_3 supports and Pt/WO_x, Pt/0.1Al-WO_x catalysts are presented in Fig. S1. The type-IV isotherms with H1 hysteresis loops indicate the uniform mesopores are formed by sphere-stack tungsten suboxide crystals in all samples, and the pore size are detected as 16.0–21.2 nm (Table 1). As

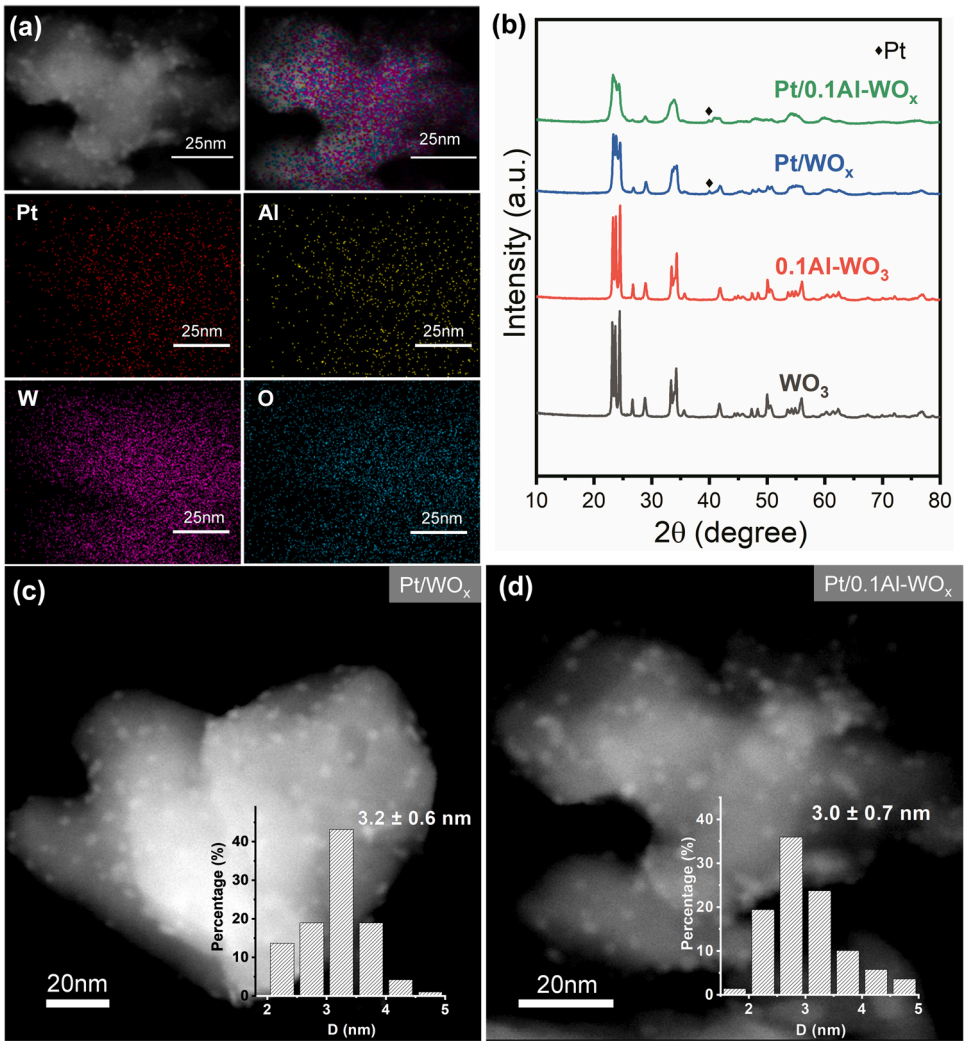

Fig. 1. The structure characterizations for samples. (a) EDS-mapping images of W, O, Pt, Al for Pt/0.1Al-WO_x; (b) XRD patterns for WO_3, 0.1Al-WO_3, Pt/WO_x and Pt/0.1Al-WO_x; STEM images for (c) Pt/WO_x and (d) Pt/0.1Al-WO_x.

also listed in Table 1, after the incorporation of a small amount of Al species, S_{BET} of tungsten oxide slightly decreases from 6.5 to 5.9 m^2/g, which suggests that AlO_x is anchored on the surface of WO_3. After Pt loading, the S_{BET} of Pt/WO_x and Pt/0.1Al-WO_x catalysts increase to 8.1 m^2/g identically, which might result from the changes of the surface structure and properties of tungsten oxide when supported Pt species. In addition, from the SEM images of WO_3 and 0.1Al-WO_3 in Figs. S2a, b, d, e, the morphologies of the two are consistent and in the shape of flower-sphere. The high-resolution transmission electron microscopy (HRTEM) images of WO_3 and 0.1Al-WO_3 in Figs. S2c,f shows clear lattice fringes without any distorted, which further demonstrates that the Al species are not doped into lattice while on the surface of WO_3.

The random scatters of Al signals in EDS mapping of Pt/0.1Al-WO_x indicate the highly dispersion and small amount of AlO_x on WO_x (Fig. 1a). Fig. 1b shows the XRD patterns of WO_3, 0.1Al-WO_3, Pt/WO_x and Pt/0.1Al-WO_x. In line with the EDS mapping results, the lack of peaks characteristic of AlO_x in 0.1Al-WO_3 and Pt/0.1Al-WO_x catalysts suggests Al species are highly dispersed on the WO_x and remain highly dispersed after Pt loading. Meanwhile, the weak peaks characteristic of metallic Pt in Pt/WO_x and Pt/0.1Al-WO_x indicate the small particle size

Table 2
Selective hydrogenolysis of glycerol over Pt/Al-WO_x catalysts.[a]

Entry	Catalysts	Conv. (%)	Sel. (%)					1,3-PDO Yield (%)
			1,3-PDO	1,2-PDO	1-PO	2-PO	Others[d]	
1	0.1Al-WO_3	–	–	–	–	–	–	–
2	Pt/WO_x	33.3	40.0	1.9	41.6	5.3	11.2	13.3
3	Pt/0.1Al-WO_x	49.0	54.5	2.7	27.8	8.7	5.4	26.7
4	Pt/0.05Al-WO_x	46.4	49.3	2.1	37.2	6.7	4.7	22.8
5	Pt/0.3Al-WO_x	22.6	47.0	3.8	23.6	25.1	0.5	10.6
6	Pt/0.1Al-WO_x[b]	79.0	40.6	1.4	30.3	4.4	23.3	32.1
7	Pt/0.1Al-WO_x-0.66[c]	56.3	46.4	1.6	40.1	5.2	6.7	26.1

[a]Reaction conditions: 433 K, 3.0 MPa H_2, 12 g 5 wt.% glycerol aqueous, 300 mg catalyst, stirring rate of 800 rpm, and reaction time of 12 h. [b]Reaction time of 30 h. [c]pH in the prepare process is 0.66. [d]Others include propane, ethylene glycol, ethanol, methanol, ethane and methane.

Table 3
XPS fitting results for the Pt/WO_x and Pt/0.1Al-WO_x catalysts.

Catalysts	Pt $4f_{7/2}$ BE (eV)	W $4f_{7/2}$ BE (eV)		W^{5+}/(W^{6+}+W^{5+})	Pt/W atomic ratio
	Pt^0	W^{6+}	W^{5+}		
Pt/WO_x	71.2	35.6	35.1	42%	5.7%
Pt/0.1Al-WO_x	71.3	35.6	35.1	50%	6.6%

of Pt, which are calculated by Scherrer formula to be both about 3.0 nm. High-angle annular dark-field scanning transmission electron microscopy (HAADF-STEM) images of Pt/WO_x and Pt/0.1Al-WO_x (Figs. 1c,d) confirm Pt nanoparticles with a mean diameter of 3.2 nm and 3.0 nm, respectively. In addition, Al species are not observable in STEM images, consistent with their being extremely small, even dispersed atomically.

3.2. Catalyst performance

The investigation of catalytic properties began with the hydrogenolysis of glycerol to 1,3-PDO as a prototype reaction-one of the most important reactions in the field of renewable biomass energy conversion. The catalytic results are summarized in Table 2. The data show that 0.1Al-WO_3 sample without Pt is inactive for the reaction (Table 2, Entry 1), and the Pt/WO_x sample without Al species gives a 1,3-PDO yield of 13.3% at the 33.3% glycerol conversion in a batch reactor at 433 K, 3 MPa H_2 for 12 h (Table 2, Entry 2). In contrast, the Pt/0.1Al-WO_x gives a 1,3-PDO yield twice as high as Pt/WO_x of 26.7% at 49% glycerol conversion under the same conditions (Table 2, Entry 3). The influence of reaction temperature, H_2 pressure (Table S2) and reaction time (Table 2, Entry 6) on Pt/0.1Al-WO_x catalytic performance was further investigated, and the highest 1,3-PDO yield of 32.1% was obtained. We also made the comparisons of the space time yield (STY) and the space time yield based on Pt metal (STY_{Pt}) between our Pt/0.1Al-WO_x catalyst and those reported in literatures, and the results are shown in Table S3. One can see that at the relatively low H_2 pressure, our present Pt/0.1Al-WO_x catalyst exhibits superior STY and STY_{Pt} to reported Pt-WO_x system at low-concentration of glycerol. Because Pt/WO_x and Pt/0.1Al-WO_x catalysts have comparable Pt loadings and nanoparticle sizes as well as the same WO_x support, we conclude that the enhanced catalytic activity of Pt/0.1Al-WO_x results from the presence of AlO_x species. From Table 2 Entry 2–5 and Fig. S3, with the increase of Al amount from 0 to 0.1 wt%, the glycerol conversion and 1,3-PDO selectivity continuously enhance, while further increasing Al loading to 0.3 wt% leads to a significant decrease in the conversion of glycerol and the selectivity of 1,3-PDO. These results demonstrate the crucial role of the highly dispersed, even atomically dispersed AlO_x in the Pt/WO_x catalyst for glycerol hydrogenolysis.

3.3. Importance of atomically dispersed Al species in enhancing catalytic performance

To understand the crucial role of atomically dispersed AlO_x in Pt/WO_x catalyst and identify the active site, we did a series of spectroscopic characterization for Pt/WO_x and Pt/0.1Al-WO_x catalysts. Firstly, the in-situ XPS spectra of Pt 4f and W 4f levels of Pt/WO_x and Pt/0.1Al-WO_x catalysts were conducted to investigate the electronic valence of Pt and W. The fitting results are presented in Figs. S4 and 3. The Pt 4f spectra of the two catalysts that reduced at 573 K are both ascribed to Pt^0 (Pt 4 $f_{7/2}$ Bes of ca.71.3) [22,30] (Fig. S4), which indicate Pt species are both reduced to metallic Pt completely. Despite of the identical Pt loadings, the surface Pt/W atomic ratio is substantially higher on the Pt/0.1Al-WO_x catalyst (6.6%) than on the Pt/WO_x catalyst (5.7%) (Table 3). Similarly, Wang et al. observed that the intensity of surface Pt gradually decreased when the W loading was increased because of less exposed Pt species [38]. Herein, the lager Pt/W atomic ratio of Pt/0.1Al-WO_x catalyst can be attributed to the more exposed Pt species, which may because the WO_x that is modified by Al species on the surface weakens the strong metal support interaction (SMSI) thereafter decreasing the partial encapsulation of Pt particles by the WO_x species. The weakening of SMSI and the decreasing partial encapsulation of Pt particles by the WO_x species after atomically dispersed AlO_x incorporation were further evidenced by CO adsorption DRIFTS. As shown in Fig. 2, the CO adsorption produces a band at 2083 cm^{-1}, which is assigned to CO adsorbed on the metallic Pt sites [36,38]. It can be seen that with the incorporation of atomically dispersed alumina, the intensity of the CO band increases obviously, which further demonstrates more Pt surface will be exposed when AlO_x is introduced [36,38], in line with the XPS data.

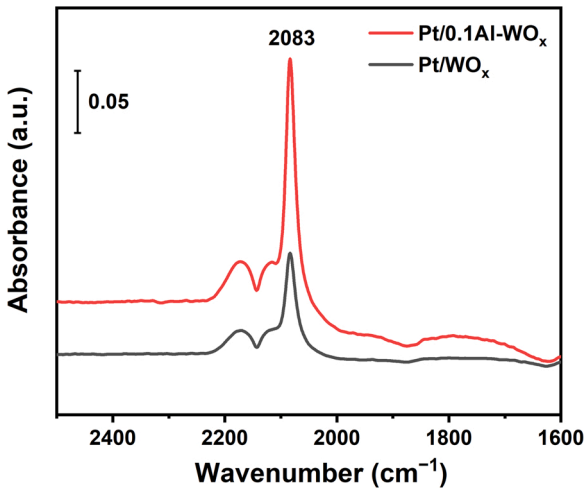

Fig. 2. DRIFTS spectra of CO adsorption on Pt/WO_x and Pt/0.1Al-WO_x catalysts.

The W4f spectra of Pt/WO_x and Pt/0.1Al-WO_x catalysts are displayed in Fig. 3. The spectra can be fitted to two groups of doublets with W$4f_{7/2}$ BEs of ca. 35.6 and 35.1 eV, which can be ascribed to W^{6+} and W^{5+}, respectively [30,41]. As listed in Table 3, the surface W^{5+}/($W5^{+}$+W^{6+}) ratio is slightly lager on the Pt/0.1Al-WO_x catalyst (50%) than that on the Pt/WO_x catalyst (42%), which suggests the W^{6+} species in Pt/0.1Al-WO_x catalyst was reduced more dramatically in H_2 than in Pt/WO_x catalyst and formed more oxygen vacancies. It also well explains the BET results, the increased S_{BET} after Pt loading of Pt/0.1Al-WO_x is larger than that of Pt/WO_x (2.2 vs 1.6 m^2/g), indicating the more oxygen vacancies in-situ generation at hydrogen atmosphere [42].

To further verify the oxygen vacancies, Raman, XRD and UV–vis were conducted for the WO_3, 0.1Al-WO_3 supports and Pt/WO_x, Pt/0.1Al-WO_x catalysts. As shown in Fig. 4a, the ν(O-W-O) modes (717 cm^{-1} and 807 cm^{-1}) in Raman spectra of WO_3 and 0.1Al-WO_3 are assigned to bridging oxygen of WO_6 octahedra [43]. It should be noted that the peak at 717 cm^{-1} is sensitive to oxygen vacancies [44]. The almost identical Raman spectra of WO_3 and 0.1Al-WO_3 supports suggests the similar surface structure of WO_3 and 0.1Al-WO_3. While comparing the Raman spectra of 0.1Al-WO_3 support with and without platinum, one can see that the loading of Pt causes the O-W-O band at 717 cm^{-1} redshifting to 709 cm^{-1} and becoming broader. This shift of Raman band can be attributed to the enhanced oxygen vacancies quantity of WO_x. Therefore, the results confirm that loading Pt species is beneficial to increase oxygen vacancies during reduction in H_2. The greater shift of the peak from 717 cm^{-1} to 709 cm^{-1} of Pt/0.1Al-WO_x catalyst than that from 717 cm^{-1} to 714 cm^{-1} of Pt/WO_x catalyst demonstrates the more oxygen vacancies are formed in Pt/0.1Al-WO_x than that in Pt/WO_x. In good agreement with the Raman results, the peaks of crystalline tungsten oxide of WO_3 and 0.1Al-WO_3 (00-024-0747) in XRD pattern (Fig. 1b) are weakened and even

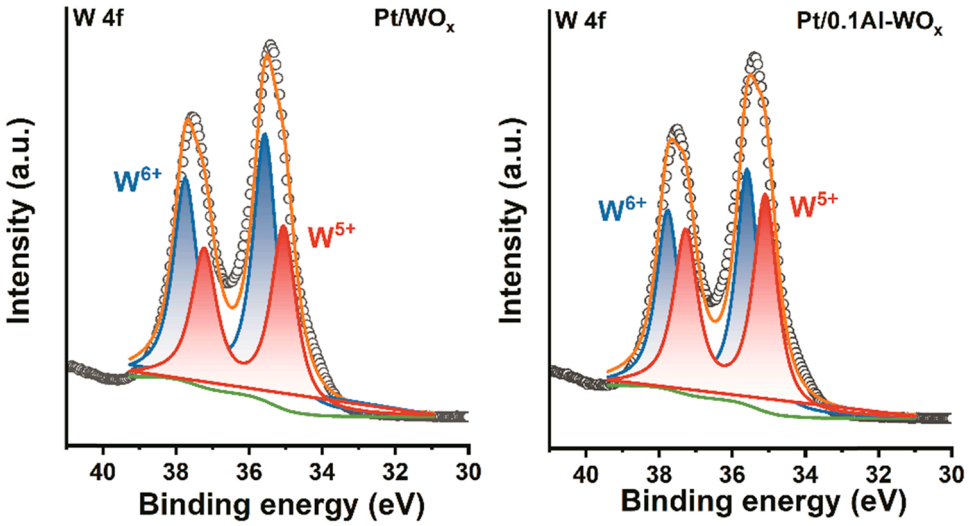

Fig. 3. In-situ XPS spectra of W 4f levels of Pt/WO_x and $Pt/0.1Al\text{-}WO_x$ catalysts.

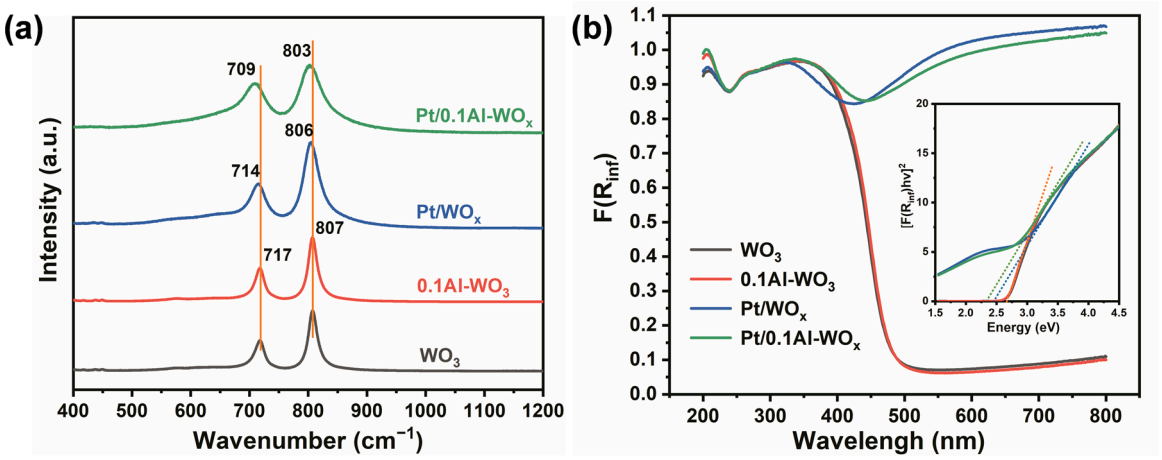

Fig. 4. Oxygen vacancies characterizations for samples. (a) Raman spectra, (b) UV–vis absorbance profiles (insert is the electronic edge energy) of WO_3, $0.1Al\text{-}WO_3$ supports and Pt/WO_x, $Pt/0.1Al\text{-}WO_x$ catalysts.

disappeared after Pt loading, which indicating the lattice oxygen was taken out after Pt loading in H_2 reduction and the tungsten oxide tended to be amorphous. Compared to the Pt/WO_x, the W species of $Pt/0.1Al\text{-}WO_x$ shows greater amorphous, which demonstrates more oxygen vacancies formation of $Pt/0.1Al\text{-}WO_x$ catalysts. Moreover, in Fig. 4b, a gradual decrease of edge (E_g) with high transmittance is observed in the UV–vis diffuse reflectance spectra of WO_3, $0.1Al\text{-}WO_3$ supports, Pt/WO_x catalyst and $Pt/0.1Al\text{-}WO_x$ catalyst, and the values of E_g are displayed in Table 1. It suggests that the electronic properties of WO_x species change because of oxygen vacancies generating, which are more conductive to delocalize the negative charge and thus increase the Brønsted acid sites with the introduction of Pt and AlO_x [45].

These results can be concluded that the oxygen vacancies are formed in tungsten oxide when Pt species are loaded, importantly, the addition of AlO_x onto Pt/WO_x results in more oxygen vacancies formation, which might be due to the more exposed Pt species by weakening SMSI after incorporation of AlO_x.

In order to further develop the in-situ generated oxygen vacancies and calculate the quantity of oxygen vacancies formation in hydrogen atmosphere, H_2-TPR was performed. In Fig. 5, all samples show double peaks before 423 K. The low-temperature peak at 295–301 K is attributed to the reduction of PtO_2, while the high-temperature one at 335 K is ascribed to that of its adjacent WO_x [21,35]. The H_2-TPR profiles show that with the increase of atomically dispersed Al content to 0.1 wt%, the high-temperature reduction peak areas (the amount of H_2 consumption) increase simultaneously, implying the facilitation of the reduction of WO_x and obtain more in-situ oxygen vacancies. These results are in line with the results of spectroscopic characterization. Moreover, it can be observed that the introduction of AlO_x does not cause appreciable shift of reduction temperature (295 K vs. 296 K), suggesting the AlO_x may not interact directly with Pt [36], the slight shift is only resulted from the weakening SMSI [38,39]. However, when Al loading up to 0.3 wt%, the dramatical decrease of reduction peak areas of WO_x indicates the high electron density of WO_x. The reduction temperature of PtO_2 shifts from 295 K to higher 301 K, which suggests the SMSI is weakened strongly due to the excessive AlO_x adding [38,39], thus leading the decrease of the reduction of WO_x. Correspondingly, XPS spectra for $Pt/0.3Al\text{-}WO_x$ also shows a dramatical decrease of the ratio for $W^{5+}/(W^{5+}+W^{6+})$ (Fig. S5). From the H_2-TPR results one can see that the reduction degree of WO_x (in-situ generated oxygen vacancies) is in good agreement with the trend of the 1,3-PDO yields. Moreover, when modulating the pH during the synthesis process of WO_x to 0.66, the resultant $Pt/0.1Al\text{-}WO_x$-0.66 catalyst exhibits the similar 1,3-PDO yield to $Pt/0.1Al\text{-}WO_x$ (Table 2, Entry 7). Consistently, the Raman and the H_2-TPR results of $Pt/0.1Al\text{-}WO_x$-0.66 catalyst in Figs. S6 and S7 shows the similar O-W-O band at 709 cm^{-1} and the similar amount of H_2 consumption with

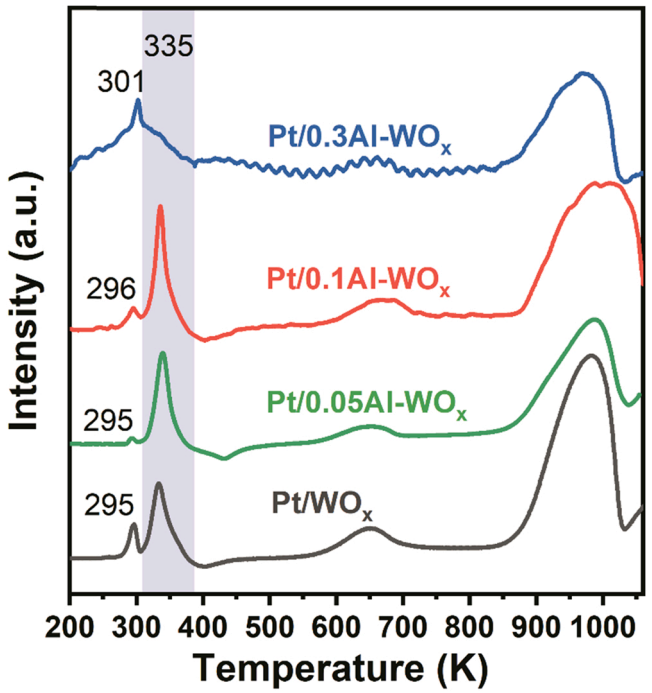

Fig. 5. H_2-TPR profiles of Pt/WO_x, $Pt/0.05Al\text{-}WO_x$, $Pt/0.1Al\text{-}WO_x$ and $Pt/0.3Al\text{-}WO_x$ catalysts.

Table 4
H_2-consumption and (3-x) values of Pt/WO_x, $Pt/0.05Al\text{-}WO_x$, $Pt/0.1Al\text{-}WO_x$, $Pt/0.3Al\text{-}WO_x$ and $Pt/0.1Al\text{-}WO_x$-0.66 catalysts.

Catalysts	H_2 consumption below 575 K ($mmol \cdot g^{-1}$)	(3-x)
Pt/WO_x	0.7	0.093
$Pt/0.05Al\text{-}WO_x$	0.9	0.130
$Pt/0.1Al\text{-}WO_x$	1.0	0.149
$Pt/0.3Al\text{-}WO_x$	0.4	0.037
$Pt/0.1Al\text{-}WO_x$-0.66	1.0	0.149

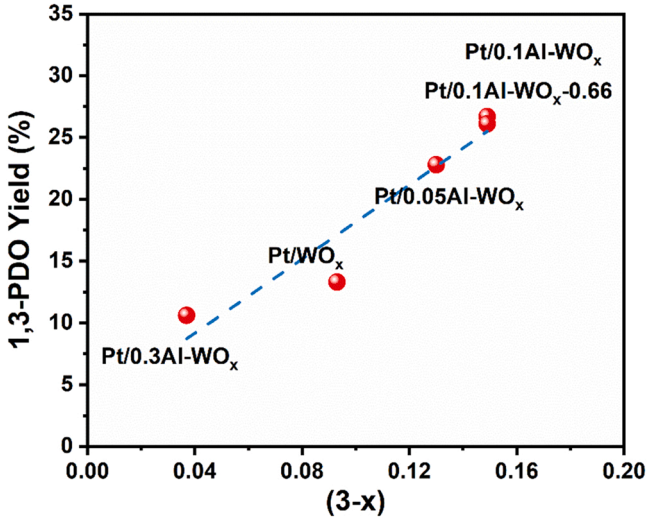

Fig. 6. Effects of (3-x) in WO_x on the yields of 1,3-PDO.

$Pt/0.1Al\text{-}WO_x$ respectively, which further verifies the relationship between the degree of WO_x reduction and 1,3-PDO yields. Since all Pt/WO_x and $Pt/Al\text{-}WO_x$ catalysts were pre-calcined at 773 K and 573 K in succession in air before H_2-TPR conduction, which have obtained

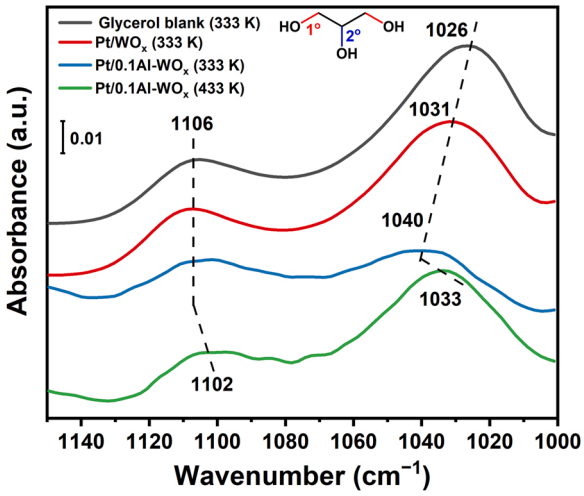

Fig. 7. The in-situ ATR-IR for the adsorption states of glycerol on Pt/WO_x and $Pt/0.1Al\text{-}WO_x$ catalysts at different temperature.

saturated oxidation state of Pt and W species, thus the quantitative description of in-situ generated oxygen defects (i.e. the (3-x) in WO_x) is attainable by calculating the H_2 consumption (Eq. 5). Accordingly, the values of calculated (3-x) are calculated and showed in Table 4. We plotted the 1,3-PDO yields as a functions of oxygen vacancies and found that a nearly line profiles was obtained (Fig. 6).

In order to further determine the generation of oxygen vacancies derived from reduction process, we conducted ^1H NMR quantitative analysis for obtained H_2O after H_2 reduction. As shown in Fig. S8 and Table S4, by using the integral area of ^1H-HMR signal as standard, the quantities of obtained H_2O for $Pt/Al\text{-}WO_x$ catalysts are calculated, consistent with the H_2 consumption from H_2-TPR results, which further confirms that the H_2 consumption contributes to the oxygen vacancies generation.

These results demonstrate that oxygen vacancies originated from reduction in hydrogen after Pt loading are crucial for achieving excellent hydrogenolysis performance. The atomically dispersed AlO_x promotes more in-situ oxygen vacancies generation by weakening SMSI resulting in the higher 1,3-PDO yields.

3.4. Catalytic mechanisms based on oxygen vacancies

In order to understand the interdependent effects of oxygen vacancies on 1,3-PDO yields and further to establish the structure-performance relationship, we conducted glycerol-adsorbed ATR-IR spectroscopy of Pt/WO_x and $Pt/Al\text{-}WO_x$ catalysts to investigate the adsorption of glycerol on the surface firstly. We prepared samples by ex-situ wet impregnation of water, and then about 1 μL glycerol aqueous solution with concentration of 5 wt.% was used for the adsorbed samples. As shown in Fig. 7, for bulk glycerol, the bands observed at 1106 and 1026 cm^{-1} are ascribed to 2° and 1° alcohol νCO bands, respectively [46,47]. After adsorption on Pt/WO_x and $Pt/0.1Al\text{-}WO_x$ catalysts at 333 K, the 1° νCO band shifts to 1031 and 1040 cm^{-1}, respectively, while the 2° νCO bands are maintained at 1106 cm^{-1}, which indicate that only the 1° hydroxyl groups is interacted with catalysts. Copeland et al. reported glycerol forms multidentate alkoxide surface species with its primary -OH on Lewis acid sites, even in the presence of bulk water. Meanwhile, the secondary -OH only interacts with basic surface oxygen atom through hydrogen bond [47]. Wang et al. observed the intensity of W═O vibrational band decreased after glycerol dropping onto the surface of WO_x by in-situ Raman spectra, demonstrating the -OH of glycerol interacted with W═O band and formed alkoxide [21]. Recently, García-Fernández et al. also confirmed that primary alkoxide is formed on the WO_x surface using ATR-IR spectroscopy [46]. Ma et al. further

Table 5
Acid content, H_2-chemisorption and Pt dispersion of Pt/WO_x and $Pt/0.1Al\text{-}WO_x$ catalysts.

Catalysts	Acid content ($mmol_{NH3}\ g_{cat}^{-1}$)	H_2-chemisorption (mmol g^{-1})	Pt dispersion (%)	
			H_2-chemisorption	STEM
Pt/WO_x	0.06	0.07	137	31
$Pt/0.1Al\text{-}WO_x$	0.11	0.09	176	33

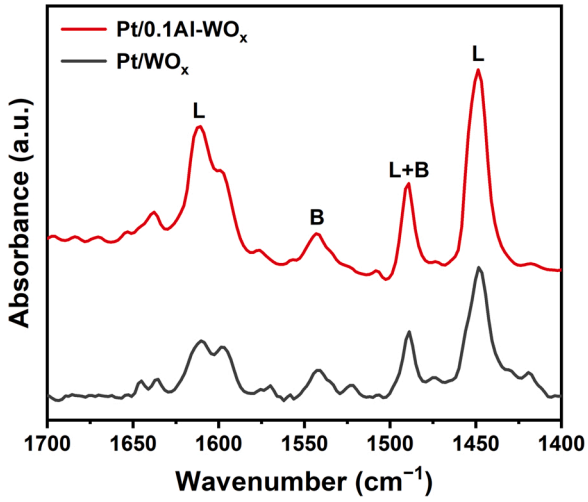

Fig. 8. Pyridine-adsorbed FT-IR spectra of Pt/WO_x and $Pt/0.1Al\text{-}WO_x$ catalysts.

pointed out that the blueshift of 1° νCO band was be assigned to the formation of primary alkoxide species on Lewis acid sites as widely mentioned, while the redshift of 2° νCO band could be assigned to the adsorption of 2° hydroxyl groups on Brønsted acid sites [31]. Therefore, in Fig. 7 the interaction of 1° hydroxyl groups is assigned to the strong adsorption on surface Lewis acid sites as alkoxide species, and the 2° hydroxyl groups don't have any interaction with catalysts at 333 K. When temperature ramps up to 433 K, the blueshift of 1° νCO is weakened and the intensity of 1° νCO becomes stronger, while a slight redshift of 2° νCO peak can be observed, confirming the weaker interaction between 1° hydroxyl groups and Lewis acid on $Pt/0.1Al\text{-}WO_x$ catalyst, but the stronger interaction between 2° hydroxyl groups and Brønsted acid on catalyst surface at higher temperature. These results are in line with the results reported by Ma and co-workers. But unlike that, such slight shift suggests little Brønsted acid sites on $Pt/0.1Al\text{-}WO_x$ catalyst thus weak adsorption of 2° hydroxyl groups on them.

As atomically dispersed Al species enhance the oxygen vacancies, the amount of Lewis acid sites should be improved correspondingly. We performed NH_3-TPD experiments to measure the variation of the acid sites (Lewis acids and Brønsted acids) on the Pt/WO_x and $Pt/0.1Al\text{-}WO_x$ catalysts surface. As shown in Table 5, the total amount of acid sites on Pt/WO_x catalyst surface increased from 0.06 $mmol_{NH3}\ g_{cat}^{-1}$ to 0.11 $mmol_{NH3}\ g_{cat}^{-1}$ when extremely small amount of Al species introduction. Compared with the glycerol-adsorbed ATR-IR spectra of the two catalysts in Fig. 7, the introduction of Al species can't change the 2° νCO peak, giving a conclusion of little surface Brønsted acid sites formation after the addition of AlO_x. On the contrary, the blueshift of 1° νCO peak can be observed obviously with atomically dispersed AlO_x introduction, which shifts from 1031 cm^{-1} on Pt/WO_x catalyst to 1040 cm^{-1} on $Pt/0.1Al\text{-}WO_x$ catalyst. Moreover, compared to Pt/WO_x catalyst, the intensity of 1° νCO bond on $Pt/0.1Al\text{-}WO_x$ catalyst decreases drastically. These results indicate a stronger interaction between Lewis acid sites of $Pt/0.1Al\text{-}WO_x$ catalyst and 1° hydroxyl groups of glycerol. As shown in Fig. S9, the 1° νCO peak of glycerol only shows a slight blueshift (2–3 cm^{-1}) on WO_3, $0.1Al\text{-}WO_3$, Pt/WO_3-cal. and $Pt/0.1Al\text{-}WO_3$-cal., which indicates little glycerol could adsorb on these four samples because of the lack of Lewis acid sites, in the form of oxygen vacancies, on WO_3. Besides, the similar shift between WO_3 and $0.1Al\text{-}WO_3$ as well as WO_3 and Pt/WO_3-cal. suggest glycerol could not adsorb on Al or Pt species. García-Fernández et al. also has proposed that the interaction between glycerol and WO_x surface is much stronger than that between glycerol and Al_2O_3 [46], thus the adsorption on AlO_x can be excluded. Hence, the stronger adsorption of 1° hydroxyl groups on $Pt/0.1Al\text{-}WO_x$ catalyst is resulted from the increased Lewis acid sites in the form of oxygen vacancies of WO_x.

In order to provide direct evidence for Brønsted and Lewis acid sites identification, we then performed pyridine-adsorbed IR spectra. As shown in Fig. 8, a strong peak at 1450 cm^{-1}, which is ascribed to typical Lewis acid sites [30,36], is observed in Pt/WO_x catalyst. And after introducing 0.1 wt.% Al species into Pt/WO_x catalyst, this band strength obviously increases. Relatively, the bands at 1540 cm^{-1}, which is ascribed to typical Brønsted acid sites [30,36], exhibits a much lower intensity, and remain constant after the addition of Al species. These results demonstrate that the acid sites measured by NH_3-TPD on Pt/WO_x and $Pt/0.1Al\text{-}WO_x$ are mainly Lewis acid sites, and the AlO_x addition is further helpful to enhance the content of Lewis acid sites, which is consistent with the glycerol-adsorbed ATR-IR results.

These results demonstrate that the addition of atomically dispersed AlO_x increases the Lewis acid sites in the form of oxygen vacancies, which facilitates the interaction with 1° hydroxyl groups of glycerol and the formation of alkoxide species, leading higher 1,3-PDO yields.

Besides the adsorption of glycerol, the origin of acid sites is crucial for identification of the glycerol hydrogenolysis mechanism and active sites. Up to now, it is generally accepted that the in-situ generated Brønsted acid sites by dissociation and spillover of H_2 are the main contributor, which is thought to have the best relationship with the 1,3-PDO yields. Ma et al. made hydrogen spillover as a function of glycerol conversion over $Pt/WO_3/ZrO_2$ catalyst and obtained a nearly linear relationship [20]. In line with this result, Wang et al. also observed a positive relationship of hydrogen spillover with the 1,3-PDO yield on $Pt/WO_x/Al_2O_3$ catalyst [38]. Moreover, they used dehydration/dehydrogenation of 2-butanol as the probe reaction to confirm the Brønsted acid sites are generated by H_2 dissociation on Pt and spillover to the neighboring WO_x. The similar conclusion has also been drawn by other groups on Pt/W-SBA-15 [22], $Pt/WO_x/T_2O_5$ [23] and $Pt/WO_3/ZrO_2$ [30] catalyst systems.

Herein, the glycerol-adsorbed ATR-IR spectra and pyridine-adsorbed FT-IR spectra have verified little intrinsic Brønsted acid sites exists in $Pt/0.1Al\text{-}WO_x$ catalyst system, the in-situ generated Brønsted acid sites need to be investigated in-depth. Thus, the chemisorption of H_2 was conducted on the Pt/WO_x and $Pt/0.1Al\text{-}WO_x$ catalysts to detect hydrogen spillover. As shown in Table 5, the $Pt/0.1Al\text{-}WO_x$ and Pt/WO_x catalysts show 0.09 mmol g^{-1} and 0.07 mmol g^{-1} H_2-chemisorption. And considering that the H_2 would be easily dissociated by $Pt/Al\text{-}WO_x$ catalysts, the H_2-chemisorption value and corresponding Pt dispersion are calculated according to the content of H atom on catalyst surface. Thus, the Pt dispersion of $Pt/0.1Al\text{-}WO_x$ and Pt/WO_x catalysts are obtained with 176% and 137%, respectively, which are much larger than the calculated Pt dispersion from STEM results (33% for $Pt/0.1Al\text{-}WO_x$ and 31% for Pt/WO_x), indicating that the hydrogen spillover occurred on Pt/WO_x and $Pt/0.1Al\text{-}WO_x$ catalysts surface [21,35,36,38]. Moreover, from the H_2-chemisorption results, there is 39% Pt dispersion discrepancy between $Pt/0.1Al\text{-}WO_x$ and Pt/WO_x, which is even larger than the both Pt dispersion results from STEM, demonstrating that $Pt/0.1Al\text{-}WO_x$ catalyst obtains the heavier hydrogen spillover than the Pt/WO_x catalyst. This result indicates that the atomically dispersed AlO_x is beneficial to the hydrogen spillover.

On one hand, considering of the encapsulation phenomenon of Pt particles by the WO_x species without AlO_x incorporation that was verified by XPS and CO-DRIFTS, the improvement of hydrogen spillover on

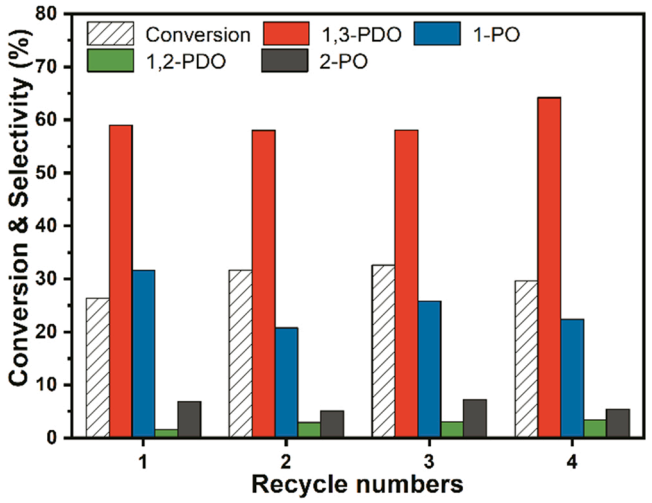

Fig. 9. Reusability test of Pt/0.1Al-WO_x catalyst for glycerol hydrogenolysis. Reaction conditions: 413 K, 3.0 MPa H_2, 12 g 5 wt.% glycerol aqueous, 300 mg catalyst, stirring rate of 800 rpm, and reaction time of 12 h.

Pt/0.1Al-WO_x catalyst can be conducted to be depended on the more exposed Pt species resulting from weaking SMSI between Pt and WO_x by AlO_x [48]. When more Pt species are exposed, the number of Pt-WO_x interface sites get expanded, which favors the hydrogen spillover to the surface of WO_x.

On the other hand, the existence of oxygen vacancies is favor for the hydrogen spillover on the WO_x surface and the transformation of hydrogen that spillover from Pt to in-situ Brønsted acid sites. Zhang and Huang et al. proposed the surface defects created solid FLP site using DFT, which can dissociate hydrogen to H^+ and H^- species easily [49]. This discover provides a direct evidence that the promotion of the oxygen vacancies for heterolytic hydrogen. Moreover, Dumesic et al. proposed the hydrogen spillover is in the form of (H^+/e^-), and the reducible support (like W^{5+}/W^{6+}, Ti^{3+}/Ti^{4+}) can facilitate the H^+ diffuse across the surface [50].

Therefore, these results demonstrate that the atomically dispersed AlO_x that associated with oxygen vacancies formation in an H_2 atmosphere can facilitate the adsorption of 1° -OH of glycerol and the in-situ generation of Brønsted acid.

3.5. Catalyst recycle

The Pt/0.1Al-WO_x catalyst was examined the stability, and the results are displayed in Fig. 9. In four runs in the hydrogenolysis of glycerol at 413 K, 3 MPa hydrogen pressure, the Pt/0.1Al-WO_x does not exhibit declining glycerol conversion and 1,3-PDO selectivity, indicating the good stability of Pt/0.1Al-WO_x catalyst. Notably, the conversion of glycerol in the second cycle increases slightly, which can be attributed to the facilitation of in-situ generated oxygen vacancies during first cycle reaction (Fig. S10). The HAADF-STEM images show that the Pt species still highly disperses on the support after cycles (Fig. S11).

Combining all the experimental and characterization results, we can present a clear picture of the function of atomically dispersed AlO_x and the crucial role of WO_x. The introduction of atomically dispersed AlO_x weakens the SMSI between Pt and WO_x thus exposes more Pt species, which facilitates the oxygen vacancies of WO_x that near Pt species in-situ formation. The selective hydrogenolysis of glycerol is benefits from the oxygen vacancies formed, which on one hand increases the adsorption of 1° hydroxyl groups of glycerol in the form of alkoxide; on the other hand improves hydrogen spillover and in-situ Brønsted acid sites generation. These results reveal the importance of the reduction degree (unsaturated coordination structure) of WO_x and the new strategy for selective hydrogenation of glycerol by employing atomically dispersed AlO_x promotion (Fig. 10). We can deduce the reaction mechanism as below (Fig. 11). The 1° hydroxyl groups of glycerol are adsorption on the Lewis acid sites that is in the form of surface oxygen defects. Hydrogen molecules are activated on the Pt metal surface and dissociated into hydrogen atoms. The hydrogen atoms spillover onto WO_x and travel through the WO_x via W^{6+} and W^{5+} exchanges, finally reduce the WO_x to form the Brønsted acid sites. The 2° hydroxyl groups of glycerol interact with in-situ Brønsted acid sites and dehydrate to form the secondary carbenium ion, which could be hydrogenated by the H^- species by the redox of low-valence WO_x.

4. Conclusion

In summary, this work proposes a strategy to improve the catalytic performance of Pt/WO_x catalyst for glycerol hydrogenolysis by atomically dispersed AlO_x introduction, and more importantly, demonstrates the origin of activity and selectivity of tungsten oxide related with the enhanced oxygen vacancies. It is found that modulating the content of atomically dispersed AlO_x will suitably weaken the SMSI between metal Pt and support WO_x for the most abundant of oxygen vacancies generation in tungsten oxide, thus optimizing the in-situ Brønsted acid sites and the adsorption of 1° -OH in glycerol for remarkably enhanced hydrogenolysis performance. The Pt/WO_x catalyst modified by atomically dispersed AlO_x promoter enhances the glycerol conversion and 1,3-PDO selectivity, simultaneously. The resulting 1,3-yield of glycerol hydrogenolysis over Pt/0.1Al-WO_x catalyst reaches as high as 32.1%, which elevates the performance of Pt/WO_x catalyst over 2 times. This discovery not only demonstrates the great potential of atomically dispersed AlO_x as highly potential promoter, but also for the first time establishes the relationship of the oxygen vacancies of WO_x with 1,3-

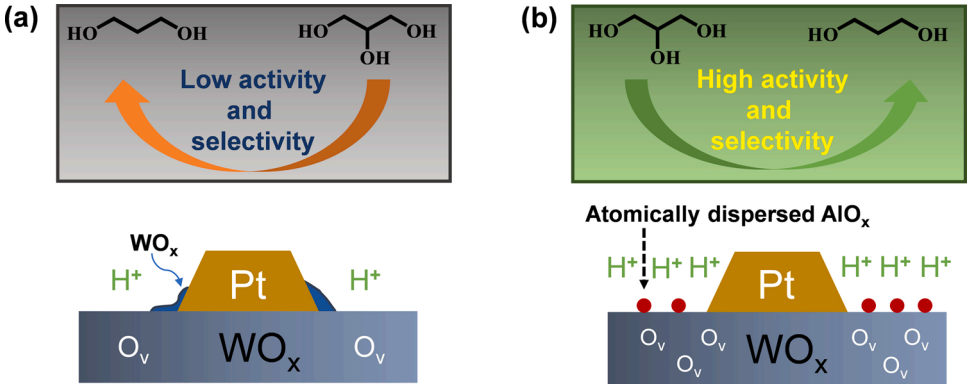

Fig. 10. Model of catalysts with and without atomically dispersed AlO_x. (a) Pt/WO_x catalyst in the hydrogenolysis of glycerol with low activity and selectivity; (b) Pt/0.1Al-WO_x catalyst in the hydrogenolysis of glycerol with high activity and selectivity simultaneously.

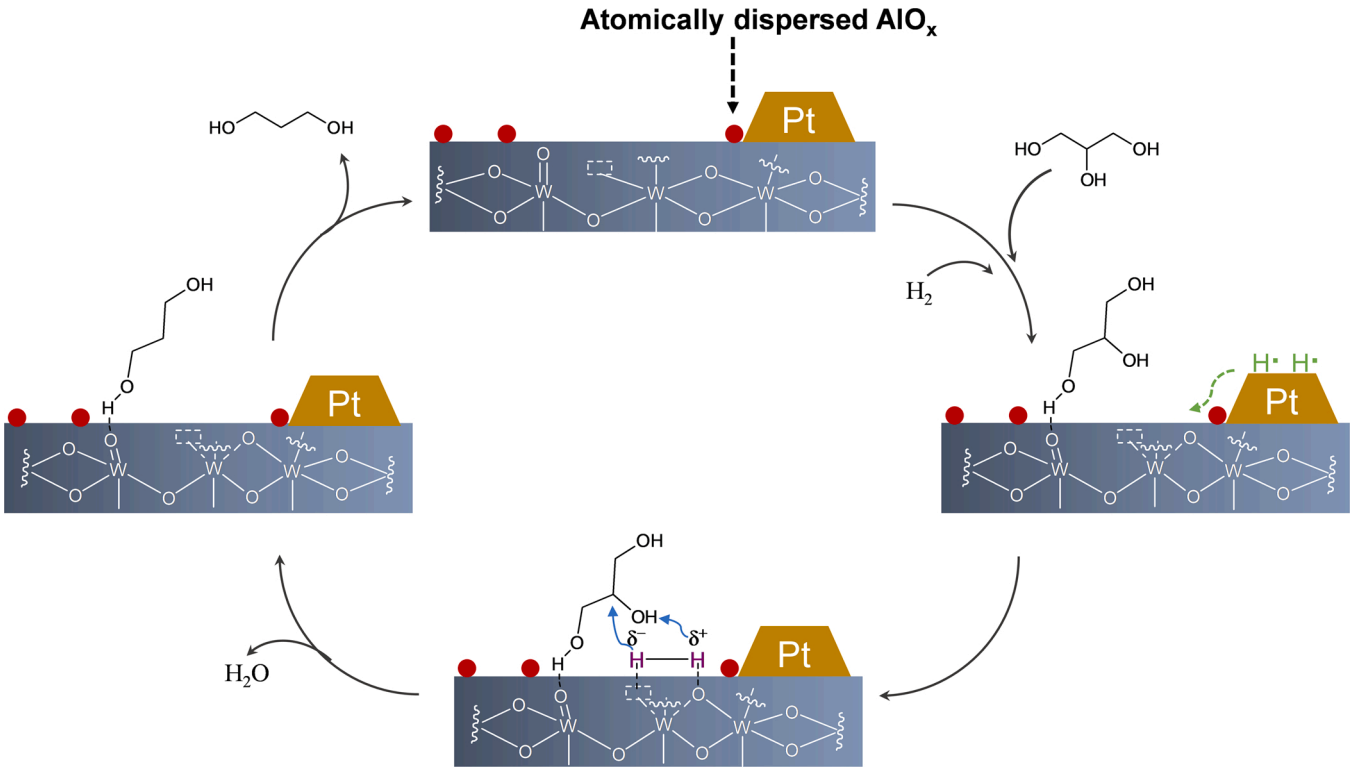

Fig. 11. Proposed possible mechanism of hydrogenolysis of glycerol to 1,3-PDO on the surface of Pt/WO_x that modified by atomically dispersed AlO_x.

PDO yields, which reveals the crucial role of the unsaturated coordination structure of WO_x in the hydrogenolysis of glycerol. This understanding will help to guide the rational design of efficient catalyst via defect engineering for the selective cleavage of secondary C—O bonds in a wide spectrum of biomass molecules, which provides a brand-new route for sustainable chemistry.

CRediT authorship contribution statement

Man Yang: Supervision, Project administration, Investigation, Writing – review & editing, Funding acquisition. **Keying Wu:** Methodology, Visualization, Investigation. **Shaodong Sun:** Investigation, Writing – review & editing. **Yujing Ren:** Supervision, Project administration, Writing – review & editing, Funding acquisition.

Declaration of Competing Interest

The authors declare that they have no known competing financial interests or personal relationships that could have appeared to influence the work reported in this paper.

Acknowledgements

The authors wish to acknowledge the support of National Natural Science Foundation of China (NSFC No. 22002118), Natural Science Foundation of Shaanxi Province (No. 2021JQ-468), Natural Science Foundation of Shaanxi Provincial Department of Education (No. 21JP086), Postdoctoral Research Foundation of China (No. 2020M683528, 2020TQ0245).

Appendix A. Supporting information

Supplementary data associated with this article can be found in the online version at doi:10.1016/j.apcatb.2022.121207.

References

[1] D. Sun, Y. Yamada, S. Sato, W. Ueda, Glycerol hydrogenolysis into useful C3 chemicals, Appl. Catal. B Environ. 193 (2016) 75–92.
[2] J. Shan, Y. Xue, D. Wang, Z. Chen, S. Zhu, Direct production of ethanol with high yield from glycerol via synergistic catalysis by Pd/CoO_x and Cu/SBA-15, Appl. Catal. B Environ. 302 (2022), 120870.
[3] L. Xu, Z. Han, Q. Yao, J. Deng, Y. Zhang, Y. Fu, Q. Guo, Towards the sustainable production of pyridines via thermo-catalytic conversion of glycerol with ammonia over zeolite catalysts, Green Chem. 17 (2015) 2426–2435.
[4] Y. Wang, S. Furukawa, S. Song, Q. He, H. Asakura, N. Yang, Catalytic production of alanine from waste glycerol, Angew. Chem. Int. Ed. 59 (2020) 2289–2293.
[5] Z. Zhang, G.W. Huber, Catalytic oxidation of carbohydrates into organic acids and furan chemicals, Chem. Soc. Rev. 47 (2018) 1351–1390.
[6] B. Tabah, A. Varvak, I.N. Pulidindi, E. Foran, E. Banin, A. Gedanken, Production of 1,3-propanediol from glycerol via fermentation by Saccharomyces cerevisiae, Green Chem. 18 (2016) 4657–4666.
[7] Y. Nakagawa, Y. Shinmi, S. Koso, K. Tomishige, Direct hydrogenolysis of glycerol into 1,3-propanediol over rhenium modified iridium catalyst, J. Catal. 272 (2010) 191–194.
[8] C. Deng, X. Duan, J. Zhou, X. Zhou, W. Yuan, S.L. Scott, Ir-Re alloy as a highly active catalyst for the hydrogenolysis of glycerol to 1,3-propanediol, Catal. Sci. Technol. 5 (2015) 1540–1547.
[9] D.D. Falcone, J.H. Hack, A.Yu Klyushin, A. Knop-Gericke, R. Schlögl, R.J. Davis, Evidence for the bifunctional nature of Pt–Re catalysts for selective glycerol hydrogenolysis, ACS Catal. 5 (2015) 5679–5695.
[10] K. Tomishige, Y. Nakagawa, M. Tamura, Selective hydrogenolysis and hydrogenation using metal catalysts directly modified with metal oxide species, Green Chem. 19 (2017) 2876–2924.
[11] L. Liu, T. Asano, Y. Nakagawa, M. Gu, C. Li, M. Tamura, K. Tomishige, Structure and performance relationship of silica-supported platinum-tungsten catalysts in selective C-O hydrogenolysis of glycerol and 1,4-anhydroerythritol, Appl. Catal. B Environ. 292 (2021), 120164.
[12] L. Liu, T. Asano, Y. Nakagawa, M. Tamura, K. Okumura, K. Tomishige, Selective hydrogenolysis of glycerol to 1,3-propanediol over rhenium-oxide-modified iridium nanoparticles coating rutile titania support, ACS Catal. 9 (2019) 10913–10930.
[13] S. Cheng, Y. Fan, X. Zhang, Y. Zeng, S. Xie, Y. Pei, G. Zeng, M. Qiao, B. Zong, Tungsten-doped siliceous mesocellular foams-supported platinum catalyst for glycerol hydrogenolysis to 1,3-propanediol, Appl. Catal. B Environ. 297 (2021), 120428.
[14] F. Wu, H. Jiang, X. Zhu, R. Lu, L. Shi, F. Lu, Effect of tungsten species on selective hydrogenolysis of glycerol to 1,3-propanediol, ChemSusChem 14 (2021) 569–581.
[15] J. Wang, M. Yang, A. Wang, Selective hydrogenolysis of glycerol to 1,3-propanediol over Pt-W based catalysts, Chin. J. Catal. 41 (2020) 1311–1319.

[16] L. Liu, Y. Zhang, A. Wang, T. Zhang, Mesoporous WO_3 supported Pt catalyst for hydrogenolysis of glycerol to 1,3-propanediol, Chin. J. Catal. 33 (2012) 1257–1261.

[17] S. Zhu, X. Gao, Y. Zhu, Y. Zhu, X. Xiang, C. Hu, Y. Li, Alkaline metals modified Pt-$H_4SiW_{12}O_{40}/ZrO_2$ catalysts for the selective hydrogenolysis of glycerol to 1,3-propanediol, Appl. Catal. B Environ. 140–141 (2013) 60–67.

[18] R. Arundhathi, T. Mizugaki, T. Mitsudome, K. Jitsukawa, K. Kaneda, Highly selective hydrogenolysis of glycerol to 1,3-propanediol over a boehmite-supported platinum/tungsten catalyst, ChemSusChem 6 (2013) 1345–1347.

[19] S. García-Fernández, I. Gandarias, J. Requies, M.B. Guemez, S. Bennici, A. Auroux, P.L. Arias, New approaches to the $Pt/WO_x/Al_2O_3$ catalytic system behavior for the selective glycerol hydrogenolysis to 1,3-propanediol, J. Catal. 323 (2015) 65–75.

[20] W. Zhou, Y. Zhao, Y. Wang, S. Wang, X. Ma, Glycerol hydrogenolysis to 1,3-propanediol on tungstate/zirconia-supported platinum: hydrogen spillover facilitated by Pt(1 1 1) formation, ChemCatChem 8 (2016) 3663–3671.

[21] J. Wang, X. Zhao, N. Lei, L. Li, L. Zhang, S. Xu, S. Miao, X. Pan, A. Wang, T. Zhang, Hydrogenolysis of glycerol to 1,3-propanediol under low hydrogen pressure over WO_x-supported single/pseudo-single atom Pt catalyst, ChemSusChem 9 (2016) 784–790.

[22] Y. Fan, S. Cheng, H. Wang, D. Ye, S. Xie, Y. Pei, H. Hu, W. Hua, Z. Li, M. Qiao, B. Zong, Nanoparticulate Pt on mesoporous SBA-15 doped with extremely low amount of W as a highly selective catalyst for glycerol hydrogenolysis to 1,3-propanediol, Green Chem. 19 (2017) 2174–2183.

[23] B. Zhao, Y. Liang, L. Liu, Q. He, J. Dong, Discovering positively charged Pt for enhanced hydrogenolysis of glycerol to 1,3-propanediol, Green Chem. 22 (2020) 8254–8259.

[24] J. Wang, N. Lei, C. Yang, Y. Su, X. Zhao, A. Wang, Effect of promoters on the selective hydrogenolysis of glycerol over Pt/W-containing catalysts, Chin. J. Catal. 37 (2016) 1513–1519.

[25] L. Gong, Y. Lu, Y. Ding, R. Lin, J. Li, W. Dong, T. Wang, W. Chen, Selective hydrogenolysis of glycerol to 1,3-propanediol over a $Pt/WO_3/TiO_2/SiO_2$ catalyst in aqueous media, Appl. Catal. A 390 (2010) 119–126.

[26] S. Zhu, X. Gao, Y. Zhu, J. Cui, H. Zheng, Y. Li, SiO_2 promoted $Pt/WO_x/ZrO_2$ catalysts for the selective hydrogenolysis of glycerol to 1,3-propanediol, Appl. Catal. B Environ. 158–159 (2014) 391–399.

[27] M. Gu, Z. Shen, L. Yang, B. Peng, W. Dong, W. Zhang, Y. Zhang, The effect of catalytic structure-modification on hydrogenolysis of glycerol into 1,3-propanediol over platinum nanoparticles and ordered mesoporous alumina assembled catalysts, Ind. Eng. Chem. Res. 56 (2017) 13572–13581.

[28] M. Yang, X. Zhao, Y. Ren, J. Wang, N. Lei, A. Wang, T. Zhang, Pt/Nb-WO_x for the chemoselective hydrogenolysis of glycerol to 1,3-propanediol: Nb dopant pacifying the over-reduction of WO_x supports, Chin. J. Catal. 39 (2018) 1027–1037.

[29] T. Kurosaka, H. Maruyama, I. Naribayashi, Y. Sasaki, Production of 1,3-propanediol by hydrogenolysis of glycerol catalyzed by $Pt/WO_3/ZrO_2$, Catal. Commun. 9 (2008) 1360–1363.

[30] Y. Fan, S. Cheng, H. Wang, J. Tian, S. Xie, Y. Pei, M. Qiao, B. Zong, Pt-WO_x on monoclinic or tetrahedral ZrO_2: Crystal phase effect of zirconia on glycerol hydrogenolysis to 1,3-propanediol, Appl. Catal. B Environ. 217 (2017) 331–341.

[31] W. Zhou, J. Luo, Y. Wang, J. Liu, Y. Zhao, S. Wang, X. Ma, WO_x domain size, acid properties and mechanistic aspects of glycerol hydrogenolysis over $Pt/WO_x/ZrO_2$, Appl. Catal. B Environ. 242 (2019) 410–421.

[32] S. García-Fernández, I. Gandarias, Y. Tejido-Núñez, J. Requies, P.L. Arias, Influence of the support of bimetallic platinum tungstate catalysts on 1,3-propanediol formation from glycerol, ChemCatChem 9 (2017) 4508–4519.

[33] S. Feng, B. Zhao, L. Liu, J. Dong, Platinum supported on WO_3-doped aluminosilicate: a highly efficient catalyst for selective hydrogenolysis of glycerol to 1,3-propanediol, Ind. Eng. Chem. Res. 56 (2017) 11065–11074.

[34] T. Mizugaki, T. Yamakawa, R. Arundhathi, T. Mitsudome, K. Kaneda, Selective hydrogenolysis of glycerol to 1,3-propanediol catalyzed by Pt nanoparticles AlO_x/WO_3, Chem. Lett. 41 (2012) 1720–1722.

[35] X. Zhao, J. Wang, M. Yang, N. Lei, L. Li, B. Hou, S. Miao, X. Pan, A. Wang, T. Zhang, Selective hydrogenolysis of glycerol to 1,3-propanediol: manipulating the frustrated Lewis pairs by introducing gold to Pt/WO_x, ChemSusChem 10 (2017) 819–824.

[36] B. Wang, F. Liu, W. Guan, A. Wang, T. Zhang, Promoting the effect of Au on the selective hydrogenolysis of glycerol to 1,3-propanediol over the $Pt/WO_x/Al_2O_3$ catalyst, ACS Sustain. Chem. Eng. 9 (2021) 5705–5715.

[37] G. Miao, L. Shi, Z. Zhou, L. Zhu, Y. Zhang, X. Zhao, H. Luo, S. Li, L. Kong, Y. Sun, Catalyst design for selective hydrodeoxygenation of glycerol to 1,3-propanediol, ACS Catal. 10 (2020) 15217–15226.

[38] N. Lei, X. Zhao, B. Hou, M. Yang, M. Zhou, F. Liu, A. Wang, T. Zhang, Effective hydrogenolysis of glycerol to 1,3-propanediol over metal-acid concerted $Pt/WO_x/Al_2O_3$ catalysts, ChemCatChem 11 (2019) 3903–3912.

[39] S. Zhu, X. Gao, Y. Zhu, Y. Li, Promoting effect of WO_x on selective hydrogenolysis of glycerol to 1,3-propanediol over bifunctional Pt-WO_x/Al_2O_3 catalysts, J. Mol. Catal. A Chem. 398 (2015) 391–398.

[40] W. Zhou, Y. Li, X. Wang, D. Yao, Y. Wang, S. Huang, W. Li, Y. Zhao, S. Wang, X. Ma, Insight into the nature of Brönsted acidity of Pt-$(WO_x)_n$-H model catalysts in glycerol hydrogenolysis, J. Catal. 388 (2020) 154–163.

[41] B. Zhao, Y. Liang, L. Liu, Q. He, J. Dong, Facilitating Pt−WO_x species interaction for efficient glycerol hydrogenolysis to 1,3-propanediol, ChemCatChem 13 (2021) 3695–3705.

[42] G. Ou, Y. Xu, B. Wen, R. Lin, B. Ge, Y. Tang, Y. Liang, C. Yang, K. Huang, D. Zu, R. Yu, W. Chen, J. Li, H. Wu, L. Liu, Y. Li, Tuning defects in oxides at room temperature by lithium reduction, Nat. Commun. 9 (2018) 1302.

[43] J. Yan, T. Wang, G. Wu, W. Dai, N. Guan, L. Li, J. Gong, Tungsten oxide single crystal nanosheets for enhanced multichannel solar light harvesting, Adv. Mater. 27 (2015) 1580–1586.

[44] T. Zheng, W. Sang, Z. He, Q. Wei, B. Chen, H. Li, C. Cao, R. Huang, X. Yan, B. Pan, S. Zhou, J. Zeng, Conductive tungsten oxide nanosheets for highly efficient hydrogen evolution, Nano Lett. 17 (2017) 7968–7973.

[45] W. Zhou, N. Soultanidis, H. Xu, M.S. Wong, M. Neurock, C.J. Kiely, I.E. Wachs, Nature of catalytically active sites in the supported WO_3/ZrO_2 solid acid system: a current perspective, ACS Catal. 7 (2017) 2181–2198.

[46] S. Garcia-Fernandez, I. Gandarias, J. Requies, F. Soulimani, P.L. Arias, B. M. Weckhuysen, The role of tungsten oxide in the selective hydrogenolysis of glycerol to 1,3-propanediol over $Pt/WO_x/Al_2O_3$, Appl. Catal. B Environ. 204 (2017) 260–272.

[47] J.R. Copeland, I.A. Santillan, S.M. Schimming, J.L. Ewbank, C. Sievers, Surface interactions of glycerol with acidic and basic metal oxides, J. Phys. Chem. C 117 (2013) 21413–21425.

[48] K. Chen, S. Koso, T. Kubota, Y. Nakagawa, K. Tomishige, Chemoselective hydrogenolysis of tetrahydropyran-2-methanol to 1,6-hexanediol over rhenium-modified carbon-supported rhodium catalysts, ChemCatChem 2 (2010) 547–555.

[49] S. Zhang, Z. Huang, Y. Ma, W. Gao, J. Li, F. Cao, L. Li, C. Chang, Y. Qu, Solid frustrated-Lewis-pair catalysts constructed by regulations on surface defects of porous nanorods of CeO_2, Nat. Commun. 8 (2017) 15266.

[50] J. He, S.P. Burt, M. Ball, D. Zhao, I. Hermans, J.A. Dumesic, G.W. Huber, Synthesis of 1,6-hexanediol from cellulose derived tetrahydrofuran-dimethanol with Pt-WO_x/TiO_2 catalysts, ACS Catal. 8 (2018) 1427–1439.